High Power Laser Science and Engineering, (2025), Vol. 13, e46, 8 pages.
doi:10.1017/hpl.2025.31

HIGH POWER LASER SCIENCE AND ENGINEERING

RESEARCH ARTICLE

Ten-megawatt-level peak power Mamyshev oscillator enabled by anti-resonant hollow-core fiber

Shan Wang[1,2,3], Di Lin[1,2,3], Xin Zhang[4], Ziheng Zhuang[1,2,3], Weijia Luo[1,2,3], Cong Zhang[1,2,3], Meng Xiang[1,2,3], Jianping Li[1,2,3], Songnian Fu[1,2,3], Pu Wang[4], and Yuwen Qin[1,2,3]

[1]*Institute of Advanced Photonics Technology, School of Information Engineering, Guangdong University of Technology, Guangzhou, China*

[2]*Key Laboratory of Photonic Technology for Integrated Sensing and Communication, Ministry of Education, Guangdong University of Technology, Guangzhou, China*

[3]*Guangdong Provincial Key Laboratory of Information Photonics Technology, Guangdong University of Technology, Guangzhou, China*

[4]*Institute of Laser Engineering, Beijing Engineering Research Center of Laser Applied Technology, Beijing University of Technology, Beijing, China*

(Received 2 December 2024; revised 6 March 2025; accepted 2 April 2025)

Abstract

Mamyshev oscillators (MOs) demonstrate extraordinarily superior performance compared with fiber laser counterparts. However, the realization of a fully fiberized, monolithic laser system without pulse degradation remains a key challenge. Here we present a high-energy MO using large mode area Yb-doped fiber and fiber-integrable interferometric super-Gaussian spectral filters that directly generates a nearly diffraction-limited beam with approximately 9.84 W average power and 533 nJ pulse energy. By implementing pre-chirp management with anti-resonant hollow-core fiber (AR-HCF), the adverse effects of super-Gaussian filtering on pulse quality are effectively mitigated, enabling pulse compression to 1.23 times the transform limit. Furthermore, AR-HCF is employed to provide negative dispersion to compensate for the positive chirp of output pulses, resulting in approximately 37 fs de-chirped pulses with approximately 10 MW peak power. This approach represents a significant step toward the development of monolithic fiber lasers capable of generating and flexible delivery of sub-50-fs pulses with tens of megawatts peak power.

Keywords: anti-resonant hollow-core fiber; fiber pulse compression; Mamyshev oscillator; pre-chirp management

1. Introduction

Mode-locked fiber lasers have been attracting considerable interest in various industrial and scientific fields due to their robust operation, compact size, high optical efficiency and cost effectiveness[1]. A critical challenge encountered by these systems is the enhancement of peak power, necessitating the achievement of higher pulse energies and shorter pulse durations. However, the intrinsic properties of fiber lasers, particularly their tight mode confinement and extended propagation length, lead to significantly nonlinear effects that ultimately destabilize pulse evolution, thereby restricting the achievable peak power to levels considerably lower than those attainable with bulk solid-state lasers. Over the past few decades, researchers have developed several advanced techniques to effectively manage these nonlinearities, including dispersion-managed fiber lasers[2], self-similar fiber lasers[3] and all-normal dispersion fiber lasers[4]. These strategies typically yield maximum pulse energies of approximately 20 nJ with sub-100-fs pulse durations in single-mode fibers (SMFs)[4]. Recent advancements in fiber-based Mamyshev oscillators (MOs) have exhibited markedly superior performance compared to other fiber-based systems, especially in their capability to directly generate megawatt-level peak power pulses from SMF oscillators[5]. Moreover, the incorporation of specially designed ultra-low numerical aperture (NA) large mode area Yb-doped fiber (LMA-YDF) and Yb-doped photonic crystal fiber (YD-PCF) has facilitated the achievement of pulse energies exceeding 1 μJ, with externally compressed pulse durations of approximately 50 fs and peak powers surpassing 10 MW. This advancement represents an order of magnitude improvement over traditional mode-locked fiber lasers[6,7].

Correspondence to: D. Lin and Y. Qin, School of Information Engineering, Guangdong University of Technology, Guangzhou 510006, China. Emails: dilin@gdut.edu.cn (D. Lin); qinyw@gdut.edu.cn (Y. Qin)

The exceptional performance of MOs can be primarily attributed to the parabolic pulse evolution, in conjunction with the step-like effective saturable absorber created by the integration of two central-wavelength-offset bandpass filters. This configuration facilitates the generation of stable mode-locked pulses even under the condition of an accumulated nonlinear phase shift of approximately 60π[5]. The Gaussian-shaped transmission profile of the spectral filters plays a pivotal role in scaling pulse energies and achieving high-quality pulse compression, generally resulting in compressed pulse durations around 1.6 times the transform-limited (TL) duration at microjoule-scale pulse energies[6,7]. However, the implementation of Gaussian-shaped filters typically necessitates the incorporation of a diffraction grating, along with a collimator and a section of SMF, resulting in a cumbersome configuration that is impractical for fiber integration. Consequently, compactly fiber-integrated interferometric spectral filters featuring a near-super-Gaussian transmission profile have become a common choice in fully fiberized MOs. Nevertheless, these MOs generally exhibit inferior performance compared to those employing Gaussian-shaped spectral filters. For instance, an MO utilizing a 10 μm core diameter polarization-maintaining Yb-doped fiber (PM-YDF) in conjunction with Gaussian-shaped spectral filters is capable of generating stable pulses with energies of 190 nJ, further compressed to 35 fs (~1.25 times the TL duration), achieving a peak power of 3 MW[8]. In contrast, an MO employing super-Gaussian filters with an equivalent core diameter of PM-YDF produces pulses of only approximately 83 nJ, compressed to 56 fs (~2.8 times the TL duration) with a peak power of 1.15 MW[9]. This performance penalty indicates the incomplete parabolic pulse evolution associated with the latter configuration. The superior performance of Gaussian-shaped filters can be attributed to their smoother spectral transmission profile, which facilitates parabolic pulse evolution more effectively. It is well established that optimizing pre-chirp is essential for accelerating pulse evolution toward an asymptotic parabolic regime within self-similar fiber amplifiers, allowing for high-quality pulse compression[10–12]. Given that pulse evolution is inherently dependent on the amplifier gain parameters, the optimal pre-chirp is contingent upon pulse energies. For example, a nearly TL 38 fs pulse with minimal pedestal at a pulse energy of 1.2 μJ has been achieved from a negatively pre-chirped self-similar YDF amplifier[13]. In conventional MOs that comprise two cascaded YDF amplifiers, it is essential that the pulses within each amplifier evolve toward a parabolic shape. Therefore, it is anticipated that the implementation of pre-chirp management within MOs could potentially benefit the evolution of pulses into a parabolic shape with a linear chirp even when employing super-Gaussian filters. In addition, a recent study shows that effective intracavity pre-chirp management can improve the achievable pulse energy in the MO[14].

The output pulses from MOs typically exhibit a slight positive linear chirp over their broadband spectrum, which is commonly compensated for through the utilization of a bulky grating-based compressor to achieve sub-50-fs pulses with megawatt-level peak powers. However, numerous applications, such as micro-machining[15], *in vivo* and *in situ* nonlinear imaging[16–18] and microsurgery[19,20], demand the flexible delivery of high-peak-power femtosecond pulses over several meters of optical fiber with minimal attenuation and distortion at the target. This capability is especially critical in contexts like laser surgery, where the laser source may need to be positioned at a considerable distance from the operational site to provide a more organized and efficient working environment for surgeons. Therefore, the development of a fiber-based compressor capable of effectively delivering microjoule-scale pulse energies over several meters while maintaining sub-50-fs pulse durations at the fiber output is highly desirable for advancing monolithic MOs.

Conventional solid-core fibers, including LMA fibers and solid-core PCFs, have been utilized for pulse compression; however, their applicability is fundamentally constrained to pulse energies of only a few nanojoules due to strong nonlinear effects and low material damage thresholds[21,22]. In contrast, advanced microstructured hollow-core fibers (HCFs) offer a highly promising alternative. The ambient air-filled cores of HCFs exhibit nonlinearities approximately two orders of magnitude lower than those of silica glass. In addition, HCFs support fundamental mode operation with a larger effective mode area and possess a significantly higher damage threshold due to their extremely low mode overlap with surrounding silica structures. These properties make HCFs particularly well-suited for both pulse compression and the flexible transmission of high-peak-power femtosecond pulses. Notably, recent investigations into photonic-bandgap HCFs and Kagome-style HCFs have demonstrated remarkable results in the realm of self-compression, achieving few-cycle pulses with energy levels reaching hundreds of microjoules, across wavelengths from ultraviolet to mid-infrared[23-25]. However, the necessity for bulky gas chambers remains a major limitation, significantly undermining the operational flexibility of these systems.

For ultrafast pulses with relatively low pulse energies, the implementation of negative dispersion in air-filled HCFs to directly compensate for the intrinsic positive chirp of laser pulses offers a more straightforward and efficient strategy for pulse compression, while minimizing nonlinear effects. This approach not only simplifies pulse compression but also enables the flexible transmission of high-peak-power femtosecond pulses. Significant efforts have been dedicated to developing monolithic ultrafast laser systems that incorporate air-filled HCF pulse compressors, allowing for the direct generation of femtosecond pulses with durations of hundreds of femtoseconds and peak powers of sub-megawatts[18,26,27].

https://doi.org/10.1017/hpl.2025.31 Published online by Cambridge University Press

Recent advancements in anti-resonant hollow-core fibers (AR-HCFs) have demonstrated both a reduction in mode overlap with the surrounding glass structures to approximately between 10^{-4} and 10^{-5} and a flattening of the anomalous dispersion profile around 1 μm. In addition, these fibers exhibit remarkably low transmission losses, typically below 1 dB/km around 1 μm[28–30]. These characteristics make AR-HCFs highly promising candidates for such applications.

In this paper, we present a high-energy MO based on commercially available PM LMA-YDF, incorporating several unique design elements that yield exceptional pulse performance. Instead of using conventional bulky grating-based Gaussian-shaped spectral filters typically employed to form an effective saturable absorber, we incorporate more compact, fiber-integrable interferometric spectral filters. To address the challenges associated with the super-Gaussian transmission profile in parabolic pulse evolution, pre-chirp management with optimized group delay dispersion (GDD) is implemented with the assistance of a precisely chosen length of AR-HCF. This configuration facilitates the generation of linearly chirped pulses with high pulse energy. The MO can reach an average output power of 9.84 W at a repetition rate of 18.46 MHz, corresponding to pulse energies of 533 nJ. Pulse compression is realized by transmitting the pulses through an optimized length of air-filled AR-HCF, where the positive chirp of the input pulse is effectively compensated by the matched anomalous dispersion provided by the HCF, resulting in a compressed pulse duration of approximately 37 fs and a peak power at the 10 MW level.

2. Experimental setup

The experimental setup is illustrated in Figure 1(a), including two cascaded Mamyshev fiber regenerators. The first regenerator consists of approximately 2 m of double-cladding PM-YDF (Coherent PLMA-YDF-10/125-VIII) with a core/cladding diameter of 10/125 μm, forwarded cladding-pumped by a 9 W laser diode at 976 nm. It serves as a lower-energy feedback loop for the subsequent power-scaling arm. The second regenerator comprises approximately 2.4 m of double-cladding PM-YDF (Coherent PLMA-YDF-25/250-VIII) with a core/cladding diameter of 25/250 μm, backward cladding-pumped by a 60 W laser diode at 976 nm through free-space coupling optics. The fiber's V-number at 1.03 μm is calculated to be approximately 5.1, theoretically supporting four LP mode groups (LP_{01}, LP_{11}, LP_{21} and LP_{02}). To ensure fundamental LP_{01} mode exclusive operation, the fiber is coiled with a bending diameter of 7 cm to introduce substantial losses to the higher-order modes. Numerical calculations reveal that the effective mode area of the LP_{01} mode decreases from approximately 360 μm^2 in the straight fiber to 254 μm^2 in the coiled configuration. Unlike conventional microjoule-scale MO architectures, this system employs two compact thin-film interference filters with near-super-Gaussian transmission profiles for offset bandpass filtering, centered at 1042 nm with a full width at half maximum (FWHM) of 3 nm and 1028 nm with an FWHM of 4.5 nm, respectively. The large spectral separation between the two filters results in a high modulation depth in the effective saturable absorber, thereby enabling the stable generation of high-energy pulses. In addition, a slight narrower bandwidth of the spectral filter prior to the LMA-YDF facilitates the evolution of the pulse into a parabolic shape, leading to an improvement in the quality of the compressed pulse. A free-space PM isolator (PM-ISO) and a fiberized PM-ISO ensure unidirectional laser operation. A 2×2 PM-coupler with a power ratio of 90:10 is spliced to the signal input port of the pump/signal combiner, allowing the injection of external seed pulses via the 10% port to initiate the mode-locking. In the second arm, a half-wave plate (HWP) combined with a polarization beam splitter (PBS) enables adjustable output coupling, which is set to 91% to maximize the energy of the output pulses. All solid-core fiber ends are spliced to appropriate silica endcaps with angle-polished end-facets for the ease of suppressing potential parasitic lasing.

Pre-chirp management is applied at the power-scaling arm by introducing variable lengths of AR-HCF or solid-core PM fiber (Coherent PM1060L) prior to the PM-YDF, providing either negative or positive GDD to the input pulses. Given the relatively low pulse energy after the spectral filter (~1.2 nJ), pulse propagation through the passive fiber is dominated by linear effects. The inset of Figure 1(b) shows a scanning electron microscope (SEM) cross-section image of the self-fabricated AR-HCF, featuring a core diameter of 40 μm and a cladding formed by seven capillaries (20.8 μm inner diameter and 0.62 μm membrane thickness). Figure 1(b) depicts the measured transmission loss and calculated dispersion profiles of the AR-HCF. The transmission loss remains nearly constant at approximately 0.035 dB/m from 950 to 1080 nm, with a slight increase to 0.1 dB/m at 1115 nm. The calculated second-order dispersion β_2 is negative over the wavelength range, gradually decreasing with wavelengths below 1080 nm (~–0.004 ps^2/m) and dropping more sharply to –0.012 ps^2/m at 1150 nm.

3. Results and discussion

3.1. Mamyshev oscillator characterization

A dispersion-managed mode-locked fiber laser serves as the seed source, providing an external signal to initiate the mode-locking. The seed laser exhibits a pulse duration of approximately 3 ps with a spectral bandwidth of 28 nm at the –10 dB level, sufficient to cover the passbands of two intracavity spectral filters. Seed pulses with an energy of approximately 55 pJ and a repetition rate of 26.08 MHz

https://doi.org/10.1017/hpl.2025.31 Published online by Cambridge University Press

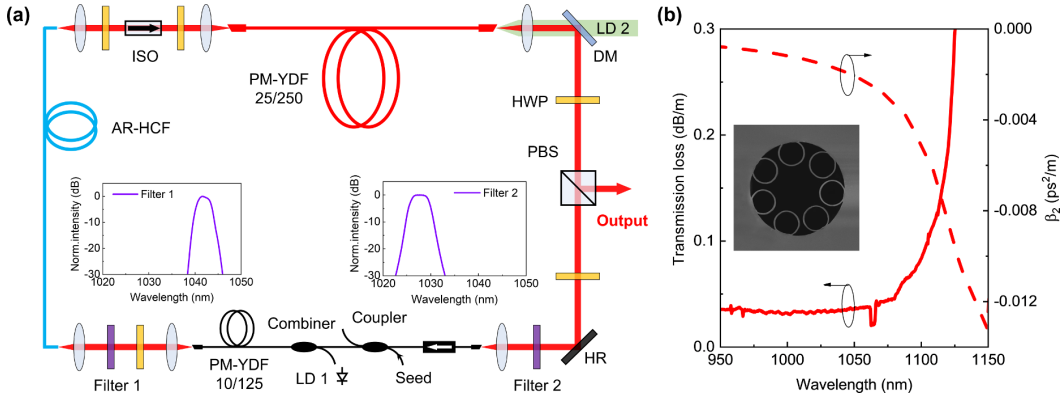

Figure 1. (a) Schematic of the experimental setup. DM, dichroic mirror; HR, high-reflection mirror; LD, laser diode. Insets: measured spectral transmission profiles of spectral filters. (b) Measured transmission loss (left-hand axis) and calculated second-order dispersion β_2 (right-hand axis) of the AR-HCF. Inset: SEM image of the fiber cross-section.

are injected into the first arm through the 10% port of the 10 dB PM-coupler. Reliable mode-locking of the MO is achieved when the absorbed pump power at the power-scaling arm is increased to approximately 11.7 W, producing single output pulses with an energy of approximately 307 nJ at a repetition rate of 18.46 MHz. Once mode-locking is established, blocking the seed pulses can further enhance the stability of the mode-locked operation.

We gradually increase the pump power of the power-scaling arm to increase the output power of the MO. Figure 2(a) depicts the average output power and the corresponding pulse energy of the output pulses as a function of absorbed pump power, revealing a slope efficiency of approximately 57% with respect to the absorbed pump power. The MO can directly generate approximately 2.3 ps chirped pulses with a maximum average power of 9.84 W, corresponding to a single-pulse energy of approximately 533 nJ. This performance is comparable to that of an MO employing the equivalent core-sized PM-YDFs with Gaussian-shaped spectral filters[31]. It is worth mentioning that the maximum achievable single-pulse energy in MOs is generally proportional to the effective mode field area (MFA) of the gain fibers within the cavity. Given that the MFA of the YDF in our study is only half that reported in Refs. [6, 7], the corresponding maximum single-pulse energy is also reduced by approximately half. Please note that the power of the first arm remains constant throughout the mode-locking process, leading to approximately 20 mW (~1.08 nJ) of spectrally filtered signal being injected into the second arm. Taking the signal coupling loss of approximately 1 dB into account, the second arm provides an effective gain of approximately 27.9 dB to achieve the maximum pulse energy. Figure 2(b) shows the measured output spectra of the second arm at variable pulse energies. As the output pulse energy increased, the spectral bandwidth at the –10 dB level gradually broadens from 66 to 89 nm (from 1005 to 1093 nm) due to the self-phase modulation (SPM)-induced spectral broadening. The spectral profiles display asymmetry,

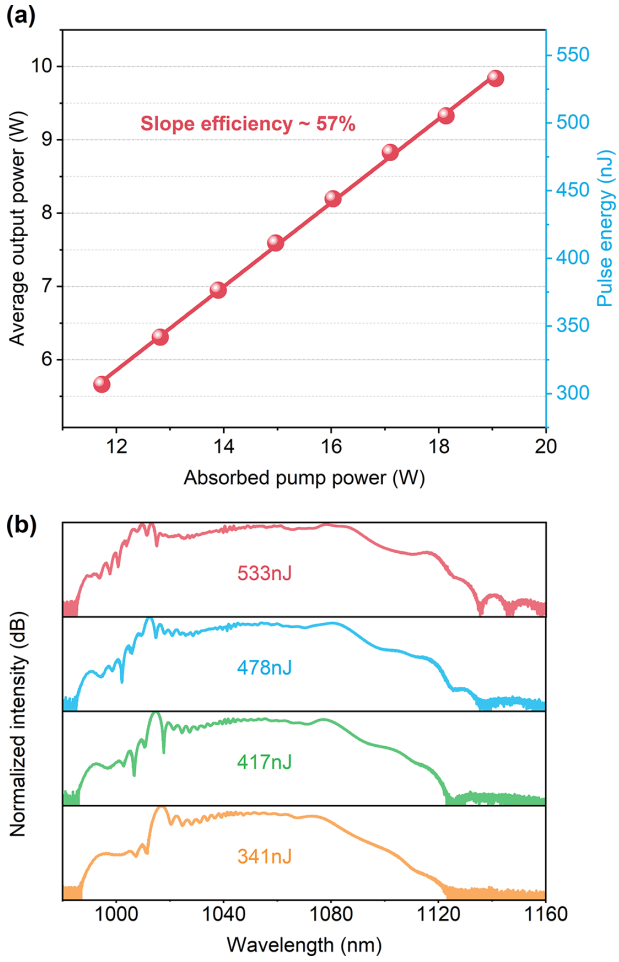

Figure 2. (a) Average output power (left-hand axis) and pulse energy (right-hand axis) as a function of absorbed pump power. (b) Measured output spectra for the indicated pulse energies.

primarily resulting from the self-steepening effect and pulse distortion induced by the third-order dispersion.

Figure 3(a) shows a typical pulse train with a repetition rate of 18.46 MHz, recorded by an oscilloscope (Lecroy WaveMaster 816Zi-B). The temporal stability of the output

https://doi.org/10.1017/hpl.2025.31 Published online by Cambridge University Press

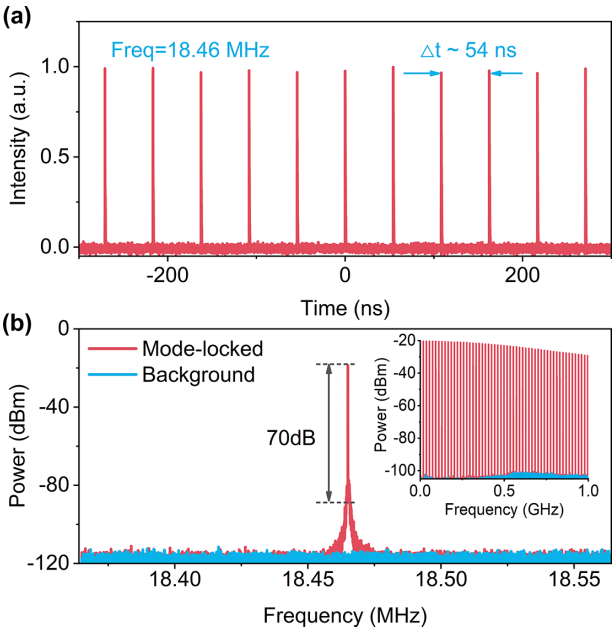

Figure 3. (a) Oscilloscope trace of the output pulses. (b) RF spectrum with an RBW of 10 Hz and a span of 200 kHz at the fundamental frequency of 18.46 MHz. Inset: RF spectrum with 1 GHz span.

pulse train is further analyzed with a radio frequency (RF) spectrum analyzer (R&S FSW50). Figure 3(b) depicts the corresponding RF spectrum measured over a frequency span of 200 kHz, with a resolution bandwidth (RBW) of 10 Hz, showing an FWHM linewidth of approximately 40 Hz and a signal-to-noise ratio of approximately 70 dB, manifesting highly stable mode-locking with low pulse jitter. The inset of Figure 3(b) shows the RF spectrum measured over a 1 GHz span with a 100 Hz RBW, revealing no evidence of multiple pulsing.

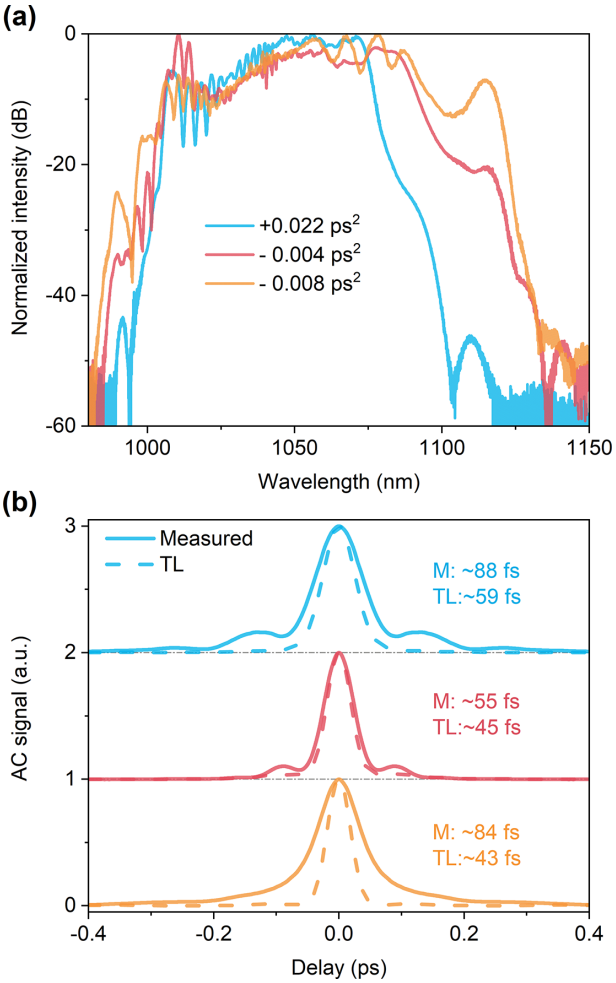

Figure 4. (a) Measured output spectra of the MO for GDD values of +0.022 ps^2 (blue), –0.004 ps^2 (red) and –0.008 ps^2 (orange) at the maximum pulse energy. (b) Corresponding measured AC traces of the de-chirped pulses (solid curve) compared to the calculated AC traces of the TL pulses (dashed curve).

3.2. Pre-chirp management

Each arm of the MO operates as a self-similar pulse amplifier, wherein the input pulse parameters play a crucial role in determining the characteristics of the output pulses. By precisely tailoring input parameters, such as pulse duration, spectral profile and pulse energy, the output pulses can be optimized to achieve maximal peak power after compression. Various experimental studies have demonstrated that pre-chirping the seed pulse can accelerate the convergence toward the parabolic regime in YDF amplifiers, thereby producing high-quality compressed output pulses. Accordingly, it is expected that applying pre-chirp to the power-scaling arm of the MO will be advantageous for generating linearly chirped output pulses at high pulse energies. In contrast to the conventional approach of employing a bulky diffraction grating pair to introduce pre-chirp in free space, which is impractical for all-fiber configurations, this work utilizes optical fibers of variable lengths to introduce controlled amounts of GDD. A 1 m long PM1060L fiber with a core diameter of 10 μm is positioned before the power-scaling arm to provide a GDD of approximately 0.022 ps^2. In contrast, 2 and 4 m long AR-HCFs are used to provide GDD values of approximately –0.004 and –0.008 ps^2, respectively. It is noteworthy that nonlinear effects within these passive fiber sections are negligible due to the relatively low pulse energy of approximately 1.2 nJ, particularly in the case of AR-HCF. Figure 4(a) shows the measured output spectra at the maximum pulse energy of approximately 533 nJ for three experimental scenarios. The broader spectrum is observed at lower GDD values, which can be attributed to the accumulation of greater nonlinear phase shifts in the shorter-duration input pulses, leading to enhanced spectral broadening caused by SPM.

The output pulses are externally compressed by a pair of transmission gratings (1000 lines/mm) with a compression efficiency of approximately 83%, resulting in a

https://doi.org/10.1017/hpl.2025.31 Published online by Cambridge University Press

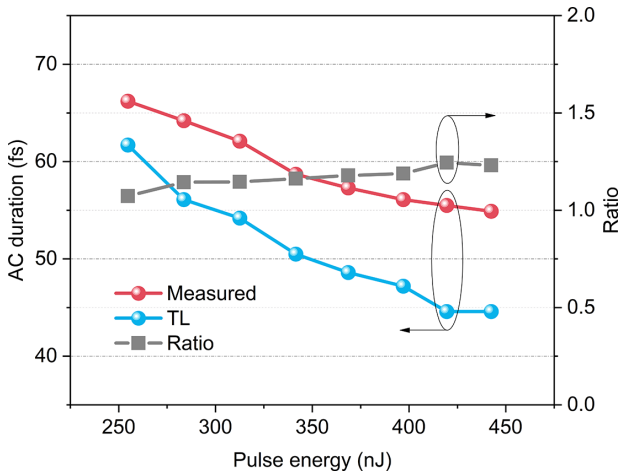

Figure 5. Measured AC duration of the de-chirped pulses (red), calculated AC duration of the TL pulses (blue) and the corresponding ratio between the two (gray) as a function of increasing pulse energy.

maximum de-chirped pulse energy of approximately 442 nJ. Figure 4(b) depicts the measured intensity auto-correlation (AC) traces of the compressed output pulses for these three scenarios. The minimum AC duration is measured as approximately 55 fs when a GDD of approximately –0.004 ps^2 is applied. This corresponds to an AC duration that is approximately 1.23 times that of the TL pulse, indicating the generation of linearly chirped pulses. To the best of our knowledge, this represents the lowest ratio achieved in MOs employing super-Gaussian spectral filters, and it even surpasses the performance observed in most cases based on Gaussian spectral filters. Despite the presence of a minor pedestal, the AC trace can be accurately fitted with a series of individual Gaussian pulses, allowing for an estimation that approximately 84% of the total pulse energy is contained within the main pulse. Assuming a Gaussian-shaped pulse, the duration of the de-chirped pulse is approximately 39 fs, corresponding to a peak power of approximately 9.7 MW. As shown in Figure 4(b), even a slight variation of GDD results in a substantial increase in the AC duration, revealing that the quality of pulse compression is highly sensitive to the GDD applied to the pulses seeding the power-scaling arm of the MO. Figure 5 illustrates the measured AC duration of de-chirped pulses at different compressed pulse energies. The AC duration decreases with the growing pulse energy due to the broadened output spectrum. In addition, the ratio of AC duration to that of the TL pulse exhibits a slight increase from 1.07 to 1.23 with a growing pulse energy, which can be attributed to the greater accumulation of uncompensated nonlinear phase shifts.

3.3. Pulse compression using an AR-HCF

We further investigate the potential of AR-HCF for ultrashort pulse compression, with a schematic of the experimental setup shown in Figure 6. The commonly used grating pair is replaced with an AR-HCF of the same type used within the cavity, providing anomalous dispersion to compensate for the positive chirp of the MO output pulses. Based on the pulse compression results achieved by the use of grating pair described in the above section, the GDD required to compress the output pulses at the maximum pulse energy of approximately 533 nJ is around –0.0235 ps^2. Consequently, an AR-HCF with a length of approximately 11.75 m is employed, providing nearly equivalent GDD to that of the grating pair. The output beam of the MO is first collimated to a spot size of approximately 1.4 mm, and subsequently focused to approximately 31 μm using an aspheric lens with a focal length of 32 mm to match the calculated fundamental mode field diameter of approximately 29 μm of the AR-HCF. This configuration yields a coupling efficiency of 90% when a 0.5 m long AR-HCF is involved. The approximately 11.75 m long AR-HCF is loosely coiled with a bending diameter of approximately 50 cm, yielding a maximum compressed pulse energy of 432 nJ with an average output power of approximately 8.0 W at the fiber output, corresponding to an overall efficiency of approximately 81%. It indicates that the transmission loss is approximately 0.04 dB/m, taking into account the coupling loss. However, the overall throughput efficiency can be further improved through advancements in the design and fabrication of AR-HCFs. In addition, the polarization extinction ratio (PER) of the transmitted beam decreases from approximately 13 dB to approximately 9.7 dB, which can be attributed to the inherent non-PM characteristics of the AR-HCF.

The AC trace of the de-chirped pulse is measured with an FWHM duration of approximately 53 fs, while the corresponding TL pulse exhibited an AC duration of 43 fs, as shown in the red solid curve and blue dashed line in Figure 7(a), respectively. The AC duration is approximately equivalent to that achieved with the grating pair-based compressor, indicating effective compensation of second-order dispersion by the AR-HCF. While a slight pedestal is observed in the AC trace, it is estimated that the main lobe comprises approximately 87% of the total pulse energy. Assuming a Gaussian-shaped pulse, the duration of the de-chirped pulse is estimated to be approximately 37 fs, resulting in a peak power of approximately 10 MW. If a more advanced AR-HCF with lower transmission loss is employed, this approach has the potential to achieve even higher peak power in this context. Figure 7(b) depicts the measured AC duration of the MO output pulses following propagation through the AR-HCF. It exhibits a monotonic decrease as pulse energy increases, consistent with our expectations. This phenomenon occurs because the required amount of GDD to compensate for the chirped pulses decreases as the pulse energy increases due to the gradual broadening of the spectral bandwidth.

The red curve in Figure 8(a) depicts the measured spectrum of the de-chirped pulses, which shows only slight

https://doi.org/10.1017/hpl.2025.31 Published online by Cambridge University Press

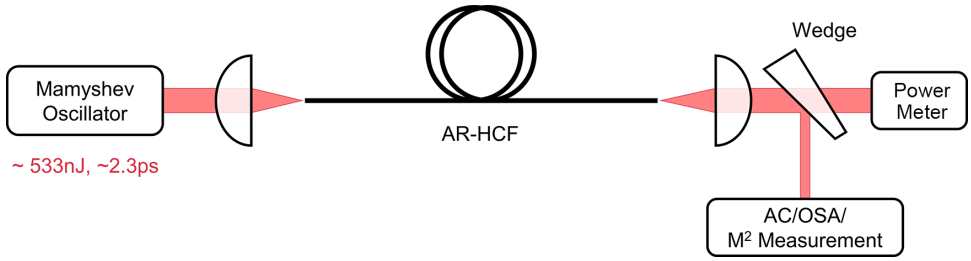

Figure 6. Schematic of the pulse compression setup utilizing the AR-HCF. OSA, optical spectrum analyzer; AC, autocorrelator.

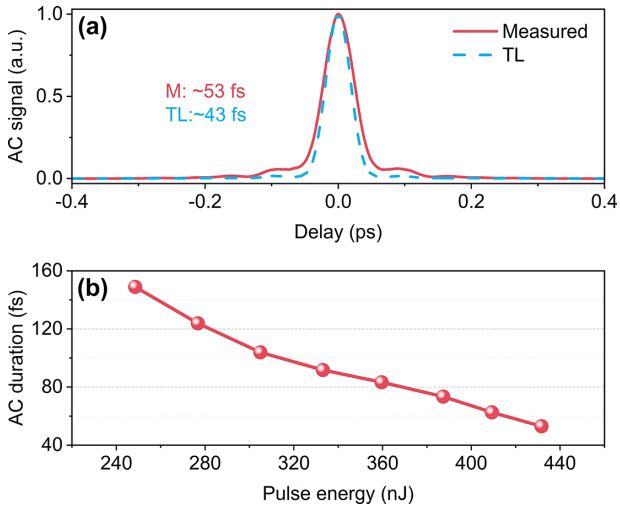

Figure 7. (a) Measured AC trace (solid red line) of the de-chirped pulse and the calculated AC trace of the TL pulse (dashed blue line) using the AR-HCF. (b) Measured AC duration of the de-chirped pulse as a function of pulse energy transmitted through the AR-HCF.

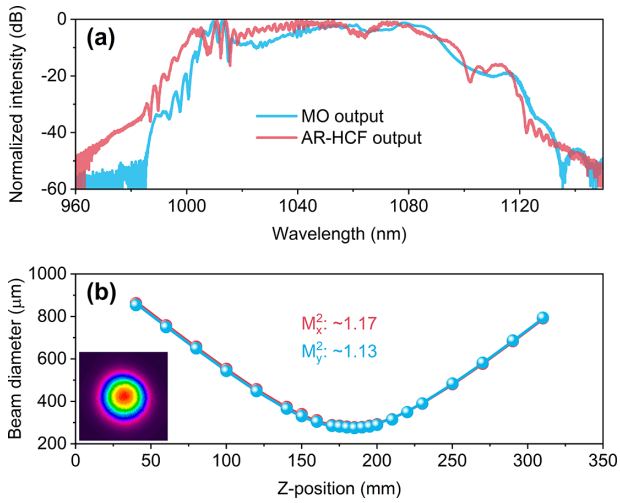

Figure 8. (a) Output spectrum of the MO (blue) and after AR-HCF delivery (red). (b) M^2 (beam quality) measurement at maximum pulse energy. Inset: measured far-field beam intensity profile.

broadening compared to that of the MO output pulses, shown with the blue curve. The close resemblance between both spectra suggests that the pulses experience only subtle nonlinear effects during the compression process. Figure 8(b) presents the beam quality (M^2) measurements at maximum pulse energy for the de-chirped pulses from the AR-HCR, yielding $M_x^2 = 1.17$ and $M_y^2 = 1.13$. This result represents a slight improvement compared to the input beam ($M_x^2 = 1.18$ and $M_y^2 = 1.30$), indicating effective single-mode operation of the AR-HCF. The output beam exhibited a pronounced Gaussian-shaped intensity distribution in the far-field, as shown in the inset of Figure 8(b). Notably, no fiber damage is observed throughout the extended duration of experimental characterization. Recent studies on picosecond pulse propagation through AR-HCFs have observed that spectral broadening due to SPM and stimulated Raman scattering becomes noticeable when the transmitted pulse accumulates a nonlinear phase shift of approximately 3π[32,33]. In our experiment, the compressed pulse accumulates a nonlinear phase shift of approximately 0.8π, indicating that AR-HCFs can facilitate microjoule-level pulse compression within the linear regime, yielding peak powers in the range of several tens of megawatts. This technique is particularly advantageous for high-energy pulses generated by MOs and gain-managed fiber amplifiers, which typically exhibit broadband spectra and minimal linear chirp. Such pulses require reduced dispersion for de-chirping, allowing for shorter fiber lengths and enabling higher peak powers for a given accumulated nonlinear phase shift.

4. Conclusions

In conclusion, we have demonstrated a high-energy MO that incorporates several distinctive features, resulting in a streamlined system architecture while maintaining exceptional pulse performance. Conventional bulky grating-based spectral filters have been replaced with compact, fiber-integrable interferometric spectral filters. The deterioration in pulse compression quality, attributable to the detrimental effects of super-Gaussian spectral filters on pulse evolution, has been effectively mitigated through the pre-chirp management utilizing an appropriate length of AR-HCF. The air-filled AR-HCF, characterized by its anomalous dispersion and ultra-low nonlinearity, is further exploited as

https://doi.org/10.1017/hpl.2025.31 Published online by Cambridge University Press

an extra-cavity linear pulse compressor to compensate for the linear positive chirp of the high-energy MO output pulses. This approach facilitated the flexible delivery of sub-40-fs pulses with peak power at the 10 MW level over a fiber length of 10 m. The results of this work represent a significant step toward the realization of a fully fiberized monolithic MO capable of directly generating tens of megawatts of peak power at the fiber distal end over extended lengths. Such a laser source is expected to be highly desirable for a broad range of applications that demand the flexible delivery of high-peak-power femtosecond pulses to a designated target.

Acknowledgements

This work was supported by the National Key Research and Development Program of China (Grant No. 2022YFB2903102), the National Natural Science Foundation of China (Grant Nos. 62335004, 62035002 and U2241225) and the Guangdong Introducing Innovative and Entrepreneurial Teams of the Pearl River Talent Recruitment Program (Grant Nos. 2019ZT08X340 and 2021ZT09X004).

References

1. M. E. Fermann and I. Hartl, Nat. Photonics **7**, 868 (2013).
2. K. Tamura, E. P. Ippen, H. A. Haus, and L. E. Nelson, Opt. Lett. **18**, 1080 (1993).
3. F. Ö. Ilday, J. R. Buckley, W. G. Clark, and F. W. Wise, Phys. Rev. Lett. **92**, 213902 (2004).
4. A. Chong, W. H. Renninger, and F. W. Wise, Opt. Lett. **32**, 2408 (2007).
5. Z. W. Liu, Z. M. Ziegler, L. G. Wright, and F. W. Wise, Optica **4**, 649 (2017).
6. W. Liu, R. Y. Liao, J. Zhao, J. H. Cui, Y. J. Song, C. Y. Wang, and M. L. Hu, Optica **6**, 194 (2019).
7. D. Lin, D. Y. Xu, J. He, Y. T. Feng, Z. Q. Ren, R. Sidharthan, Y. M. Jung, S. Yoo, and D. J. Richardson, J. Lightwave Technol. **40**, 7175 (2022).
8. P. Sidorenko, W. Fu, L. G. Wright, M. Olivier, and F. W. Wise, Opt. Lett. **43**, 2672 (2018).
9. T. Wang, B. P. Ren, J. Wu, R. Su, P. Ma, Z. Luo, and P. Zhou, IEEE J. Sel. Top. Quantum Electron. **27**, 8800105 (2021).
10. H. W. Chen, J. K. Lim, S. W. Huang, D. N. Schimpf, F. X. Kärtner, and G. Q. Chang, Opt. Express **20**, 28672 (2012).
11. J. Lim, H. W. Chen, G. Q. Chang, and F. X. Kärtner, Opt. Express **21**, 4531 (2013).
12. W. Liu, D. N. Schimpf, T. Eidam, J. Limpert, A. Tunnermann, F. X. Kartner, and G. Q. Chang, Opt. Lett. **40**, 151 (2015).
13. J. Zhao, W. X. Li, C. Wang, Y. Liu, and H. P. Zeng, Opt. Express **22**, 32214 (2014).
14. J. Yan, D. Xu, D. Lin, H. C. H. Mulvad, S. M. A. Mousavi, Y. Jung, D. Richardson, F. Poletti, and L. Xu, Laser Photonics Rev. **19**, 2401910 (2025).
15. B. Debord, M. Alharbi, L. Vincetti, A. Husakou, C. Fourcade-Dutin, C. Hoenninger, E. Mottay, F. Gérôme, and F. Benabid, Opt. Express **22**, 10735 (2014).
16. M. Andreana, T. Le, W. Drexler, and A. Unterhuber, Opt. Lett. **44**, 1588 (2019).
17. A. Kudlinski, A. Cassez, O. Vanvincq, D. Septier, A. Pastre, R. Habert, K. Baudelle, M. Douay, V. Mytskaniuk, V. Tsvirkun, H. Rigneault, and G. Bouwmans, Opt. Express **28**, 15062 (2020).
18. A. Fernández, L. Grüner-Nielsen, M. Andreana, M. Stadler, S. Kirchberger, C. Sturtzel, M. Distel, L. Zhu, W. Kautek, R. Leitgeb, A. Baltuska, K. Jespersen, and A. Verhoef, Biomed. Opt. Express **8**, 3526 (2017).
19. L. Andrus, H. Jeon, M. Pawlowski, B. Debord, F. Gerome, F. Benabid, T. Mau, T. Tkaczyk, and A. Ben-Yakar, Sci. Rep. **12**, 20554 (2022).
20. K. Subramanian, I. Gabay, O. Ferhanoglu, A. Shadfan, M. Pawlowski, Y. Wang, T. Tkaczyk, and A. Ben-Yakar, Biomed. Opt. Express **7**, 4639 (2016).
21. J. W. Nicholson, S. Ramachandran, S. Ghalmi, M. R. Yan, P. Wisk, E. Monberg, and E. V. Dimarcello, Opt. Lett. **31**, 3191 (2006).
22. H. Lim, F. Ö. Ilday, and F. W. Wise, Opt. Express **10**, 1497 (2002).
23. T. Balciunas, G. Fan, S. Haessler, C. Fourcade-Dutin, T. Witting, A. A. Voronin, A. M. Zheltikov, F. Gérôme, G. G. Paulus, A. Baltuska, and F. Benabid, in *19th International Conference on Ultrafast Phenomena*, OSA Technical Digest (online) (Optica Publishing Group, 2014), paper 08. Tue.D.7.
24. J. Limpert, in *Conference on Lasers and Electro-Optics*, OSA Technical Digest (Optica Publishing Group, 2016), paper SW4I.3.
25. M. Nisoli, IEEE J. Sel. Top. Quantum Electron. **30**, 8900114 (2024).
26. X. M. Liu, J. Lægsgaard, and D. Turchinovich, Opt. Express **18**, 15475 (2010).
27. A. J. Verhoef, K. Jespersen, T. V. Andersen, L. Grüner-Nielsen, T. Flöry, L. Zhu, A. Baltuska, and A. Fernández, Opt. Express **22**, 16759 (2014).
28. H. Sakr, Y. Chen, G. T. Jasion, T. D. Bradley, J. R. Hayes, H. C. H. Mulvad, I. A. Davidson, E. N. Fokoua, and F. Poletti, Nat. Commun. **11**, 6060 (2020).
29. H. C. H. Mulvad, S. A. Mousavi, V. Zuba, L. Xu, H. Sakr, T. D. Bradley, J. R. Hayes, G. T. Jasion, E. N. Fokoua, A. Taranta, S. U. Alam, D. J. Richardson, and F. Poletti, Nat. Photonics **16**, 448 (2022).
30. M. A. Cooper, J. Wahlen, S. Yerolatsitis, D. Cruz-Delgado, D. Parra, B. Tanner, P. Ahmadi, O. Jones, Md. S. Habib, I. Divliansky, J. E. Antonio-Lopez, A. Schülzgen, and R. Amezcua Correa, Optica **10**, 1253 (2023).
31. D. Lin, D. Xu, J. He, Y. Feng, Z. Ren, and D. J. Richardson, in *Conference on Lasers and Electro-Optics Europe and European Quantum Electronics Conference*, OSA Technical Digest (Optica Publishing Group, 2021), paper cj_4_4.
32. S. A. Mousavi, H. C. H. Mulvad, N. V. Wheeler, P. Horak, J. Hayes, Y. Chen, T. D. Bradley, S. Alam, S. R. Sandoghchi, E. N. Fokoua, D. J. Richardson, and F. Poletti, Opt. Express **26**, 8866 (2018).
33. W. Lu, X. Zhang, K. Zhu, K. Du, and P. Wang, Chin. J. Lasers **49**, 0306001 (2022).

https://doi.org/10.1017/hpl.2025.31 Published online by Cambridge University Press